DOI: 10.1002/chem.200902615

Gelation-Induced Enhanced Fluorescence Emission from Organogels of Salicylanilide-Containing Compounds Exhibiting Excited-State Intramolecular Proton Transfer: Synthesis and Self-Assembly

Manoj Kumar Nayak,[b] Byung-Hwa Kim,[a] Ji Eon Kwon,[a] Sanghyuk Park,[a] Jangwon Seo,[a] Jong Won Chung,[a] and Soo Young Park*[a]

Abstract: Self-assembly structure, stability, hydrogen-bonding interaction, and optical properties of a new class of low molecular weight organogelators (LMOGs) formed by salicylanilides **3** and **4** have been investigated by field-emission scanning electron microscopy (FESEM), X-ray diffraction (XRD), UV/Vis absorption and photoluminescence, as well as theoretical studies by DFT and semiempirical calculations with CI (AM1/PECI = 8) methods. It was found that salicylanilides form gels in nonpolar solvents due to π-stacking interaction complemented by the presence of both inter- and intramolecular hydrogen bonding. The supramolecular arrangement in these organogels predicted by XRD shows lamellar and hexagonal columnar structures for gelators **3** and **4**, respectively. Of particular interest is the observation of significant fluorescence enhancement accompanying gelation, which was ascribed to the formation of J-aggregates and inhibition of intramolecular rotation in the gel state.

Keywords: fluorescence · gels · proton transfer · salicylanilides · self-assembly

Introduction

Over the past decade, low-molecular-weight organic gelators have attracted considerable interest because of their diverse applications as supramolecular soft materials.[1] Organogels are nonflowing viscoelastic materials produced by adding a small amount of organogelator (usually less than 1 wt%) to an excess of organic solvent. The formation of organogels is facilitated by highly directional self-assembly through noncovalent interactions such as electrostatic interaction,[2] intermolecular hydrogen bonding,[3] intramolecular hydrogen bonding,[4] donor–acceptor interactions,[5] and metal coordination.[6] Subsequently, higher aggregates are formed through intercomplex interactions (hydrogen bonding, π-stacking interactions, or van der Waals forces) to form the fully gelated network. Organogelators can self-assemble into various types of aggregates such as fibrils,[7] strands, and tapes.[8] These aggregates are highly entangled and cross-linked through a junction zone[9] to form a three-dimensional (3D) network that immobilizes excess solvent molecules. The organogels have many applications such as biocatalysts, hydrometallurgy, and cosmetics. Hence, intense research has focused on the synthesis and study of many types of organogelators.[10] Recently, there has been increasing interest in the development of functional gel systems with π-conjugated molecular structures due to their potential application in various optoelectronic fields, including enhanced charge transport,[11] light harvesting,[12] fluorescence, and sensing.[4a,13]

In an attempt to obtain a new functional organogelator with potential photonic applications, we have designed and synthesized photoactive organogelators containing peripheral alkyl amide for gelation and salicylanilide (2-hydroxy-*N*-phenylbenzamide) for fluorescence emission (Scheme 1). To realize a rather simple but very efficient organogelator structure, long alkyl chains with an amide group, which is

[a] B.-H. Kim, J. E. Kwon, Dr. S. Park, Dr. J. Seo, J. W. Chung, Prof. S. Y. Park
Center for Supramolecular Optoelectronic Materials and WCU Hybrid Materials Program
Department of Materials Science and Engineering
Seoul National University, ENG 445
San 56-1, Shillim-dong, Kwanak-ku, Seoul 151-744 (Korea)
Fax: (+82) 2-886-8331
E-mail: parksy@snu.ac.kr

[b] Dr. M. K. Nayak
Current address: Department of Chemistry
Texas A&M University at Qatar
PO Box 23874, Doha (Qatar)

Supporting information for this article is available on the WWW under http://dx.doi.org/10.1002/chem.200902615.

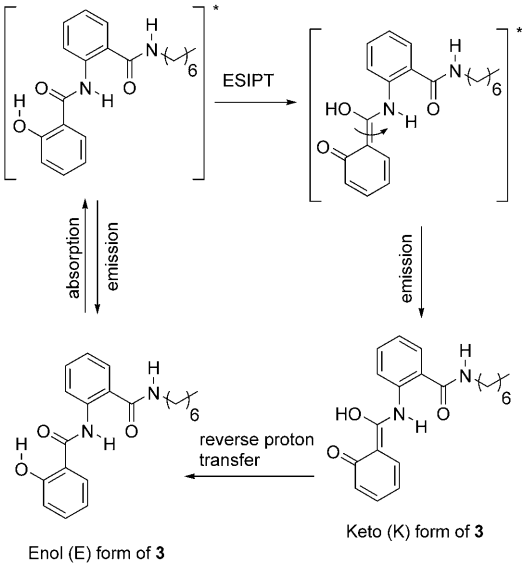

Scheme 1. Four-level photochemical and photophysical processes in an ESIPT system, represented by **3**.

widely known for its gelation power, were selected and attached to a salicylanilide part with unusual fluorescence. Fluorescence emission from salicylanilide derivatives has been widely investigated and it was concluded that the emission originates from excited-state intramolecular proton transfer (ESIPT).[14] Salicylanilides have also been the subject of extensive investigations in medicinal chemistry, due to their ability to serve as inhibitors of the protein tyrosine kinase epidermal growth factor receptor (EGFR PTK), related to cancer, psoriasis, and restenosis.[15] However, the self-assembly behavior and related properties of salicylanilide derivatives remain unexplored in the field of functional gels and supramolecular organic soft materials. Our target salicylanilide gelators (**3** and **4** in Scheme 2) were designed to undergo both intermolecular and intramolecular hydrogen bonding. As a reference compounds, we synthesized benzanilide analogues **7** and **8** to investigate the specific role of ESIPT-active salicylic hydroxyl groups in **3** and **4** in the gelation properties. We carried out SEM and XRD studies to characterize the structure of gels, and measured UV/Vis absorption and photoluminescence with specific focus on the spectroscopic difference between solution and gel states. Theoretical calculations were carried out to better understand the driving force for gelation as well as the mechanism of ESIPT emission. Structural effects of ESIPT molecules on twisted intramolecular charge transfer (TICT) induced fluorescence quenching were analyzed by means of DFT calculations.

Results and Discussion

Design principle, synthesis, and self-assembly structure of organogels: *ortho*-Substituted *N*-heptyl amide and *O*-heptyl ester derivatives of salicylanilide-containing compounds **3**, **4**, and **10** and benzanilide-type non-ESIPT analogues **7** and **8** were synthesized according to the procedure depicted in Scheme 2. The cyclized intermediate 2-hydroxyphenyl bezoxazine-4-one derivatives **1** and **2** were prepared by dehydrocyclization between salicylic acid and the corresponding anthranilic acid with triphenyl phosphite in pyridine in 20–30% yield. The coupling reaction between benzoyl chloride and the corresponding anthranilic acid in pyridine to afford 2-phenyl bezoxazine-4-one intermediates **5** and **6** proceeded in 50% yield. Subsequently, amidolysis of **1**, **2** and **5**, **6** with *n*-heptylamine in pyridine led to the final ESIPT gelator products **3**, **4** and non-ESIPT analogues **7**, **8**, in yields of 60–80%. Intermediate compound **9** was obtained by hydrolysis

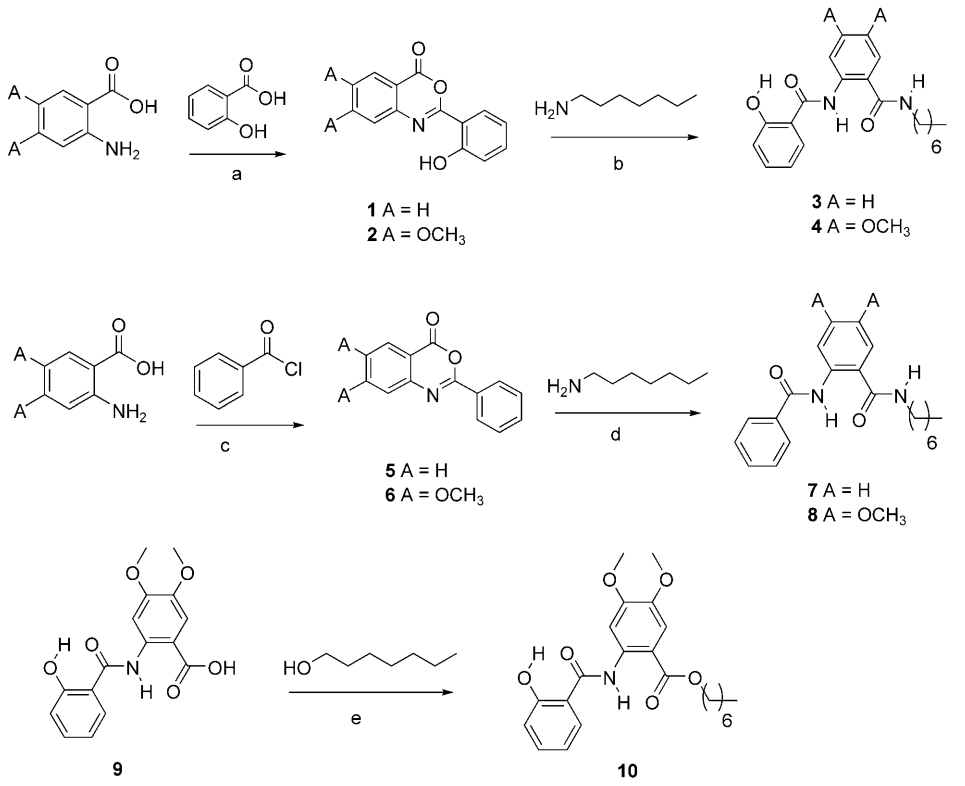

Scheme 2. Synthesis of salicylanilide-containing organogelators **3** and **4** and benzanilide-type non-ESIPT analogues **7** and **8**. a) Triphenyl phosphite, pyridine, 100°C, 2 h; b) pyridine, 100°C, 24 h; c) Pyridine, RT, 5 h; d) pyridine, 100°C, 24 h; e) triphenylphosphine, diethylazodicarboxylate (DEAD), RT, 24 h.

of **2** with aqueous potassium hydroxide and subsequently esterified with heptanol by using the Mitsunobu reagent from triphenylphosphine and diethyl azodicarboxylate to give **10** in 61% yield. The molecular structures were fully characterized by FTIR and ^{1}H NMR spectroscopy, MS-EI/HRMS, and elemental analysis.

Gelation ability was estimated in various organic solvents (Table 1). Organogelators **3** and **4** induce gelation in nonpolar solvents such as dodecane and *n*-hexane with critical gelation concentrations (CGC) as low as 0.2 wt%, but not in polar solvents. Likely, the amide bond provides the main force for gelation through intermolecular hydrogen bonding, which can be indirectly evidenced by means of model compound **10**, which has an ester bond instead of an amide bond. Indeed, model compound **10** did not immobilize solvents but formed crystals, that is, intermolecular hydrogen bonding of the alkyl amide group is an important factor for gelation. Moreover, intramolecular hydrogen bonding of the salicylanilide group in **3** and **4** is also essential to the gelation behavior, since benzanilides **7** and **8**, which lack that structural element, cannot gelate solvents but form needle- or diamond-shaped crystals. This implies that intramolecular hydrogen bonding in the salicylanilide unit contributes to a planarization effect that not only allows ESIPT but also improves π stacking for the gelation.

Table 1. Basic properties of organogels.

Compound	Form	CGC	Solvent	Transparency	T_{gel} [°C]
3	gel	0.2 wt%	*n*-hexane, dodecane	opaque	70
4	gel	0.2 wt%	*n*-hexane, dodecane	translucent	80
7	needle-shaped crystals				
8	diamond-shaped crystals				
10	needle-shaped crystals				

Considering the structures of the LMOGs prepared in this work, and the well-known fact that hydrogen bonding interaction among amide groups is one of the main driving forces for the self-assembly of organogelators in organic solvents, FTIR spectroscopy is an important tool for investigating the different noncovalent interactions involved in gelation.[16,17] To obtain structural information on self-assembled materials, FTIR spectra were measured in three different states: solution (1 wt%) in chloroform, gel (1 wt%) in *n*-hexane, and solid powder. In solution, four main characteristic peaks appeared at 3395, 2929 and 2854, 1607, and 1523 cm^{-1} for OH or amide NH asymmetric stretching (ν_{OH} or ν_{NH}), antisymmetric (ν_{as}) and symmetric (ν_s) CH_2 stretching, amide C=O stretching (ν_{CO}, amide I), and NH bending (δ_{NH}, amide II), respectively (see the spectra of **4** and **8** in Figure 1 and Figure S5 (Supporting Information);Table S1 of the Supporting Information lists band assignments). In the gel (dried gel or powdered solid) state (Figure 1) the ν_{OH} or ν_{NH}, amide I, and δ_{NH} peaks are shifted to 3390 (3312), 1604 (1600), and 1524 (1532) cm^{-1}, respectively. The redshifts of the amide I and ν_{NH} bands as well as the blueshift of the δ_{NH} band indicate that intermolecular hydrogen-bond formation occurs in the gel state. Moreover, the absence of any bands above 3400 cm^{-1} in the gel state indicates the presence of strongly hydrogen bonded NH groups in the supramolecular gel network. The NH stretching frequency of 3312 cm^{-1} in the solid state suggests the presence of strong intermolecular hydrogen-bonding association in the dried gel. Also, shifting of antisymmetric (ν_{as}) and symmetric (ν_s) CH_2 stretching frequency bands was observed from 2929 and 2854 cm^{-1} in the solution phase to 2925 and 2854 cm^{-1} in the gel state, 2925 and 2853 cm^{-1} in the solid state, respectively. The decrease in fluidity of the hydrophobic chains due to the formation of strong aggregates by van der Waals interaction is evident from this particular shift in the CH_2 stretching frequency.[17a] Thus, it is concluded that hydrogen bonding and van der Waals interaction are the major factors contributing to gelation of **3** and **4**. In contrast, in non-ESIPT analogue **8** in solution (solid) the ν_{NH} and amide I bands appear at 3367 (3418) and 1602 (1663) cm^{-1}, that is, wavenumbers typical of non-hydrogen-bonded systems[16d,17c,d] (see Figure S5 in the Supporting Information), and evidence of their nonparticipation in the aggregation processes. Further insight into the hydrogen-bonding abilities of gelators was obtained by theoretical consideration of all possible pairing modes of dimers. These calculations provide us with a more general picture of the ability to form hydrogen-bonded complexes, and the major driving force for gelation is discussed on the basis of DFT calculations (vide infra).

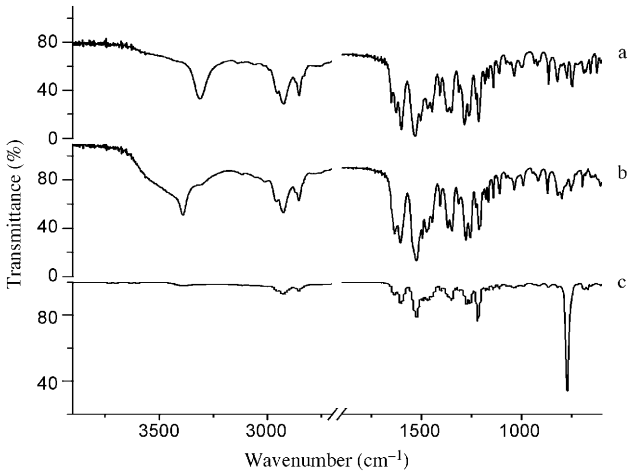

Figure 1. FTIR spectra of gelator **4** in a) solid powder, b) 1 wt% gel in *n*-hexane, and c) 1 wt% of chloroform solution.

To obtain visual insights into the aggregation mode, we observed the xerogel morphologies of *n*-hexane/dodecane

gels **3** and **4** with a field emission scanning electron microscope (FE-SEM). As shown in Figure 2, many stiff fibrillar aggregates with diameters of several tens of micrometers were observed for **3**. The SEM images of xerogel **4** showed flexible fibrillar aggregates with 100 nm diameter, which are entangled with each other to give a 3D network.

X-ray diffraction (XRD)[18] has great potential for elucidating the molecular structure of organogels and providing information about long-range ordering in the molecular self-assembly, from which a packing model of molecules in the gel phase can be proposed. Figure 3 shows the XRD pattern of the xerogel of **3** prepared in dodecane (1.0 wt %), which has three reflections at 18.40, 9.16, and 6.16 Å in the low-angle region (reciprocal spacing ratio of 1:1:1) corresponding to (100), (200), and (300) of a lamellar packing. A single XRD peak observed at 7.63 Å most likely originates from the length of the parent salicylanilide moiety without the alkyl chains. The interlamellar spacing of 18.40 Å is somewhat larger than the molecular lengths of 15.55 and 16.07 Å for gelators **3** and **4**, respectively, calculated by the AM1 method. Thus, an interdigitated arrangement of molecules in the gel is proposed to be the most plausible structure. Intermolecular alkyl-chain interdigitation leading to lamellar π stacking or hydrogen-bonding stacking of gelator **3** was assumed on the basis of these XRD studies. The X-ray diffraction pattern of the dodecane xerogel of **4** showed four low-angle reflections, at 25.00, 14.57, 12.35, and 9.42 Å (reciprocal ratio of $1:\sqrt{3}:{}^{1}/_{2}$), which correspond to columnar hexagonal packing.[19] An additional singular peak was found at 7.89 Å. Even though the chemical structure of gelator **4** is almost the same as that of **3**, the arrangement of molecules was totally different, possibly due to the two methoxyl groups. Given the different packing structures of xerogels **3** and **4**, it is apparent that the two methoxyl groups exert significant steric control on their packing modes. Because of the steric requirement of the two methoxyl groups, it seems likely that molecules of **4** can not self-assemble face-to-face. Instead, a somewhat tilted stacking structure is favored due to the two methoxyl substituents. This specific arrangement is considered to produce a columnar structure arranged in hexagonal close packing.

To investigate the driving force of self-assembly in **3** and **4**, we calculated the energies of model aggregate structures stabilized by cooperative π -stacking, hydrogen bonding, and van der Waals interactions by DFT. Three plausible isomeric dimers were built up with head-to-head intermolecular hydrogen bonding of the salicylanilide

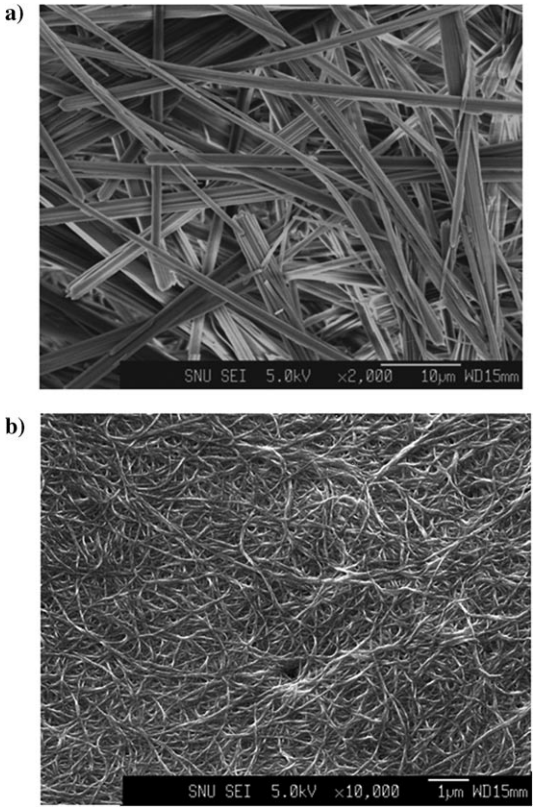

Figure 2. FESEM images of xerogels of a) **3** and b) **4**.

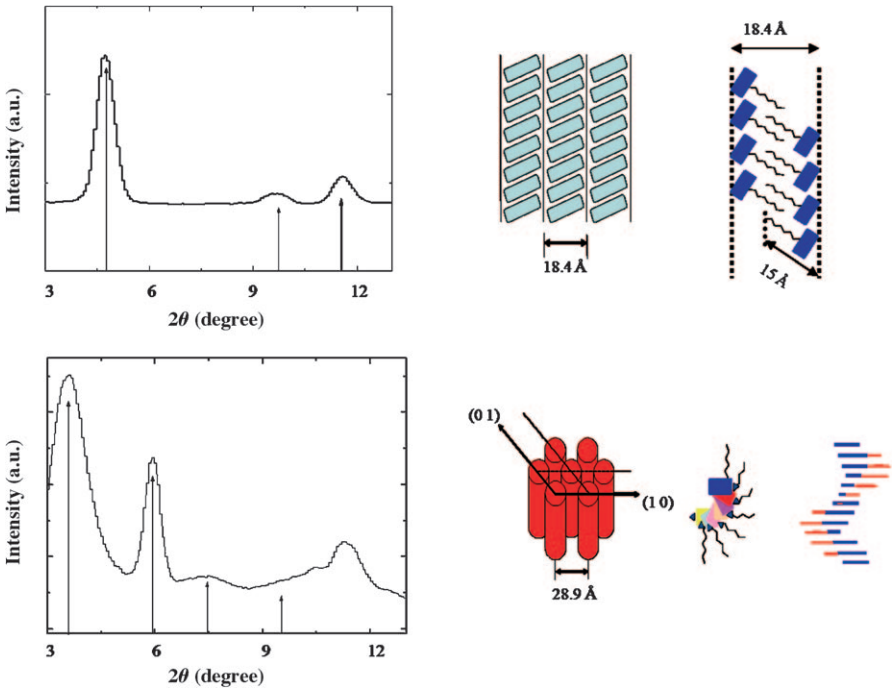

Figure 3. XRD patterns of xerogels of **3** (top), **4** (bottom), and schematic representation of arrangements in gels.

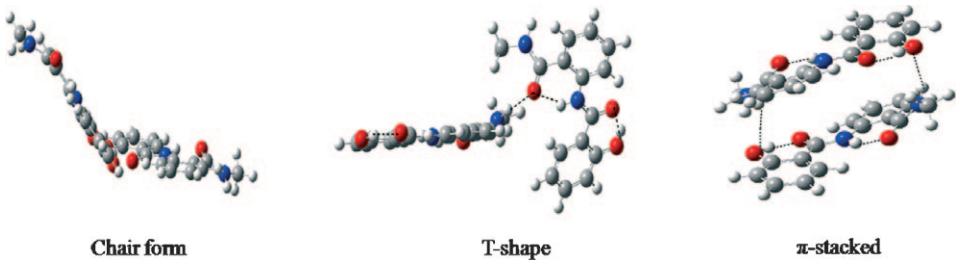

Figure 4. Fully optimized structures for all three dimer systems of gelator **3** at the B3LYP/6-31G** level of theory in the gas phase. Dark gray balls represent carbon atoms, light gray balls hydrogen, blue balls nitrogen, and red balls oxygen.

unit (chair form), tail-to-tail intermolecular hydrogen bonding of the alkyl amide unit (T shape), and head-to-tail π-stacked dimers (Figure 4). The structure and energetics of these hydrogen-bonded and stacked dimers of gelator **3** were investigated by DFT B3LYP/6-31G** computations in the gas phase (Table 2). The calculated interaction energies for the chair form, T shape, and π-stacked dimers are 3.10, 7.33, and 9.81 kcal mol^{-1}. Hence the order of stability of π-stacked > T shape > chair form also suggests the same order of gelation capability. This result implies that the gelation is primarily driven by the π-stacking interaction and is significantly assisted by inter- and intramolecular hydrogen bonding. It is noteworthy that the calculated dihedral angle of about 16–19° between two planes of π-stacked dimers favors the formation of slightly tilted geometries, as revealed by XRD studies on dodecane xerogel, such as lamellar and hexagonal columnar structures for gelators **3** and **4**, respectively. This is considered beneficial in attaining higher efficiency of fluorescence emission by favorably reducing the intermolecular vibronic interactions which would otherwise induce nonradiative deactivation processes.

Table 2. Energetic [kcal mol^{-1}] and geometric parameters of dimers (gas phase, 298.15 K).[a]

Conformer	Bond lengths [Å]	ΔE_e^{cc}	D_e^{cc}	ΔH
chair form	$O_a\cdots H-O_d$ 2.71 (inter-)	3.10	3.39	−1.9
	$O_a\cdots H-O_d$ 1.66 (intra-)			
	$O_a\cdots H-N_d$ 1.78 (intra-)			
T shape	$O_a\cdots H-N_d$ 1.98 (inter-)	7.33	8.15	−5.8
	$O_a\cdots H-O_d$ 1.65 (intra-)			
	$O_a\cdots H-N_d$ 1.81 (intra-)			
π stacked	$O_a\cdots H-N_d$ 2.18 (inter-)	9.81	10.67	−8.5
	$O_a\cdots H-O_d$ 1.59 (intra-)			
	$O_a\cdots H-N_d$ 1.75 (intra-)			

[a] ΔE_e^{cc}: binding energy, difference in electronic energies after including the counterpoise correction; D_e^{cc}: equilibrium dissociation energy, energy difference including zero-point energy and counterpoise correction; ΔH: thermodynamic corrections for enthalpy in the gas phase.

Gelation-induced enhanced fluorescence emission: To study the spectroscopic properties of self-assembled aggregates, UV/Vis absorption and photoluminescence spectra were recorded in dodecane, as it was a good gel-forming solvent. Propanol, which is miscible with dodecane, was used to disturb the intermolecular hydrogen bonding. Two samples were prepared to compare the gel to the solution state: 99.5 wt% dodecane and 0.5 wt% organogelator (gel state), and 66.3 wt% dodecane, 33.2 wt% *n*-propanol, and 0.5 wt% organogelator (solution state). Figure 5a shows the UV and PL spectra for gelator **3** and Figure 5b shows the UV and PL spectra for gelator **4**. The gel state gave a markedly broader band[10d] absorption spectrum in comparison to the solution state. The apparent absorption tail in the longer wavelength region is due to the scattering effect produced by gelation. An emission with large Stokes shift observed at 470 nm in both gel and solution state is thought to originate

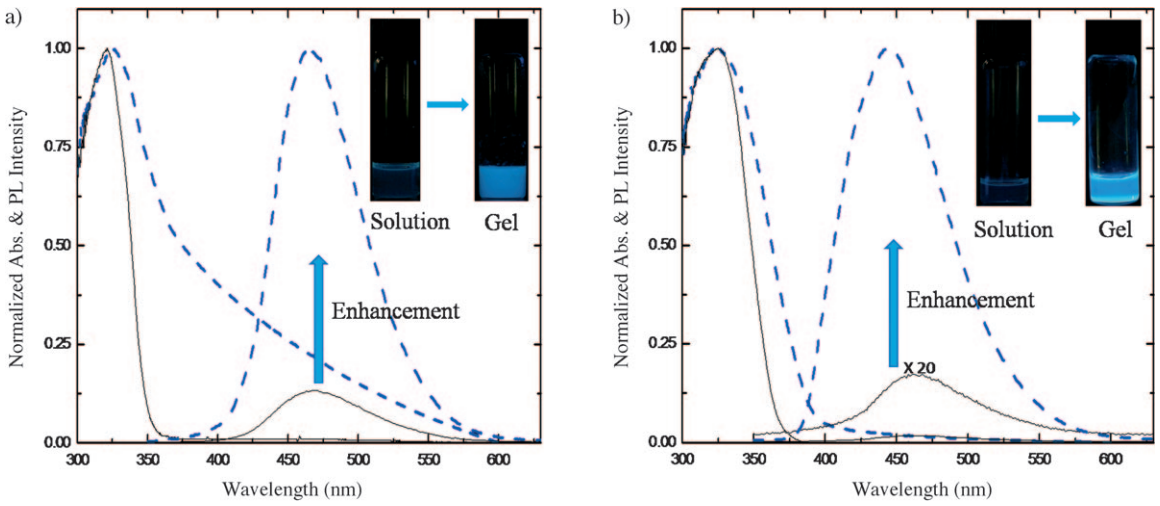

Figure 5. Normalized UV/Vis absorption and photoluminescence spectra of a) **3** and b) **4** in solution (solid line) and gel (dashed line) state.

from the proton-transferred keto (K) form of **3** shown in Scheme 1. Complete absence of enol emission suggests that the excited enol form (**3**-E*) decays mainly to the excited keto form (**3**-K*) by effective ESIPT rather than to the ground enol form (**3**-E) with normal emission in both solution and gel state, which was further confirmed theoretically (see Table 3). The intensity of photoluminescence in the gel state was sevenfold enhanced over that in the solution state. We speculate that in the solution of **3**, nonradiative decay process such as internal conversion (IC) and twisted intramolecular charge transfer (TICT) preferentially take place, as reported previously for benzanilide[20] and salicylideneaniline derivatives.[21] In contrast, it seems that these detrimental nonradiative decay processes are suppressed in the gel state because of reduced motional relaxation due to gelation. Significant fluorescence enhancement was observed to accompany gelation, which was attributed to the intermolecular stacking and inhibition of intramolecular rotation in the gel. Analogous phenomena were previously observed by others,[12b,22] whereby inhibition of intramolecular rotation and formation of J-aggregates were also shown to enhance fluorescence emission. Enhanced fluorescence emission was observed not only from the dodecane gel, but also from crystal and powdered solid states of gelators **3** and **4**. In the PL spectrum of **4**, even more dramatic fluorescence enhancement was observed compared to **3**. The PL intensity from the gel state was almost fifty times larger than that from the solution state. The fluorescence quantum efficiencies Φ_{PL} of ESIPT for gelator **3** are 0.108, 0.032, and 0.024 in cyclohexane, chloroform, and *n*-propanol, respectively, while Φ_{PL} of poly(methyl methacrylate) (PMMA) film doped with 10 wt% of **3** was 0.182. Similarly, Φ_{PL} of **4** are 0.093, 0.002, and 0.002 in cyclohexane, chloroform, and *n*-propanol, respectively, while the Φ_{PL} of 0.135 for PMMA film doped with 10 wt% of **4** indicates "rigidochromism" effected by restricted intramolecular twisting motion of the salicylanilide group in the gel or polymer film.

Table 3. Energetic characterization of keto form (**3**-K) and enol form (**3**-E) in ground (S_0) and excited (S_1) states in the gas phase.

B3LYP/6-31G**	**3**-E	**3**-K	B3LYP TD/6-31G**	**3**-E*	**3**-K*
ground state (S_0)			excited state (S_1)		
relative energy [kcal mol^{-1}]	0	13.14		5.06	0
barrier height [kcal mol^{-1}]	23.65[a]			2.39[a]	
excitation energy [nm]	325.97	411.45	emission energy [nm]	347[a]	461[a]
	314;[a] 323[b]	405[a]		–	472[b]

[a] Semiempirical AM1/PECI = 8 calculation. [b] Experimentally observed data in cyclohexane.

To further study the relationship between molecular structures and optical properties, the geometrical parameters of keto–enol tautomers and their energy-minimized, preferred conformations were calculated by DFT B3LYP/6-31G** and semiempirical calculations at the AM1/PECI = 8 level of theory. The selected parameters are summarized along with experimentally observed absorption and emission maxima in Table 3. Selected bond lengths, dihedral angles, and charge densities on the atoms involved in ESIPT, which were computed by Mulliken population analysis from optimized B3LYP geometries, are shown in Figure 6, which clearly displays a planar salicylanilide with twisted alkyl amide group. Note that the geometry of the keto form in the ground state (S_0) was optimized while keeping the O_a–H distance the same as the O_d–H distance in the optimized geometry of the enol form, where O_d and O_a refer to the donor and acceptor oxygen atoms in the enol form, respectively. Otherwise, the optimization will revert to the enol form. The calculations demonstrate that the enol form is most stable, and the keto form is 13.14 kcal mol^{-1} higher in energy. This is understandable because proton transfer in the enol form results in two OH groups being bonded to an olefinic carbon atom in the keto form. Moreover, there is partial loss of aromaticity of the benzene ring, as suggested by Sobolewski and Domcke.[23] However, in the first excited singlet state (S_1) the keto form is 5.06 kcal mol^{-1} more stable than the enol form. The AM1 calculations also predict similar results, except that the enol form is 19.47 kcal mol^{-1} more stable than the keto form in the S_0 state, whereas the keto form is 9.08 kcal mol^{-1} more stable than the corresponding enol form in the S_1 state under isolated conditions.

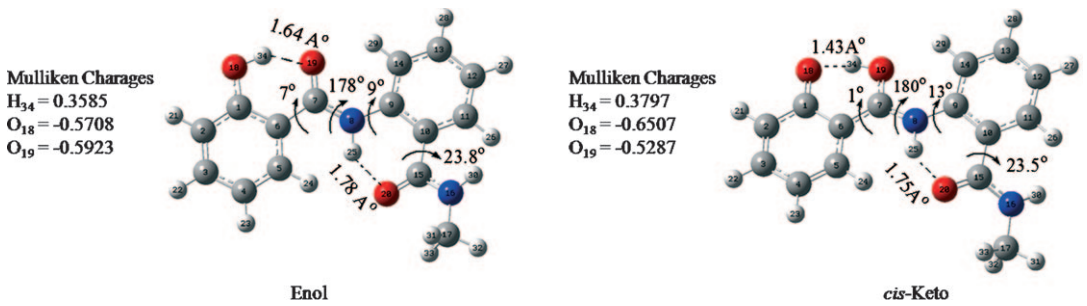

Figure 6. Optimized structure of keto–enol forms of gelator **3** at correlated DFT (B3LYP) level with 6-31G** basis set in the gas phase. Dark gray balls represent carbon atoms, light gray balls hydrogen, blue balls nitrogen, and red balls oxygen.

The transformation from enol to keto in the S_0 and S_1 states can be thought of as arising from proton transfer from O_d to O_a, with concomitant redistribution of electron density in and around the six-membered hydrogen-bonded ring. Alternatively, one could view this as a hydrogen-atom transfer. In either case, one needs to identify the "reaction coordinate" and investigate the potential-energy change along it. We chose to vary $r(O_d{-}H)$ and optimize the rest of the structural parameters for value of this parameter using the AM1/PECI=8 method (Figure 7). The resulting potential-

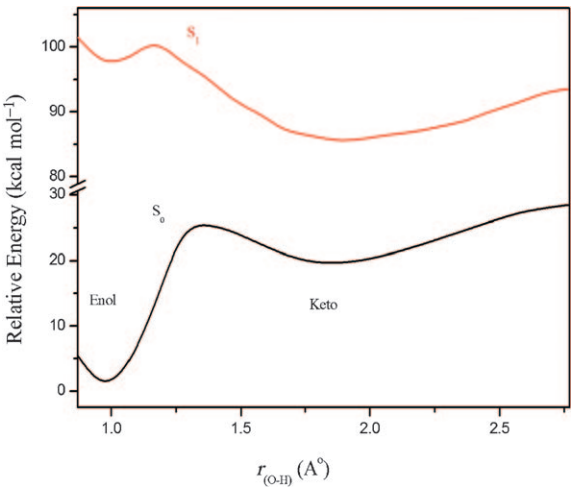

Figure 7. Potential-energy profile for intramolecular proton transfer in the ground and excited state of **3** obtained by varying $r(O_d{-}H)$ and optimizing the remaining structural parameters for each choice of $r(O_d{-}H)$ by means of AM1/PECI=8 calculation.

energy profile again reveals that the enol form is most stable in the ground state, whereas the keto form is most stable in the first excited singlet (S_1) state. The barrier of 23.65 kcal mol^{-1} for enol to keto transformation (**3**-E→**3**-K) is large enough to make ground-state intramolecular proton transfer (GSIPT) unviable under thermal conditions, whereas upon photoexcitation a much smaller **3**-E*→**3**-K*interconversion of 2.39 kcal mol^{-1} in the S_1 state allows highly efficient ESIPT to give the strongly Stokes shifted tautomer emission (10155 cm^{-1}), which is in good agreement with experimental observation (9773 cm^{-1}). After decaying to the ground state, the keto form reverts to the original enol form over the reverse proton-transfer barrier (**3**-K→**3**-E) of 5.67 kcal mol^{-1}. Moreover, the intrinsic four-level process (**3**-E→**3**-E*→**3**-K*→**3**-K→**3**-E) provides an ideal scheme for stimulated emission by easy population inversion of the proton-transferred keto form.

Figure 8 shows the geometry-dependent potential energies in the S_0 and S_1 states for the keto form of ESIPT gelator **3**. We analyzed the rotations around the three flexible bonds that can change their conformations in excited states: two aromatic amide bonds (Ar–CO and Ar–N) and the amide bond itself (N–CO) by changing geometrical parameters of interest from the optimized geometry of **3**. For twisting of

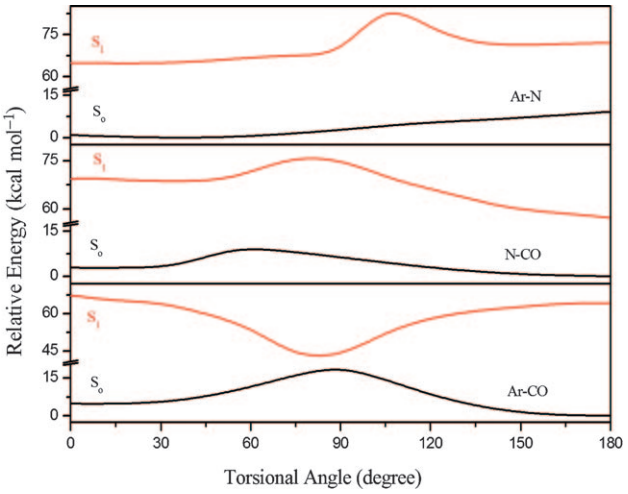

Figure 8. Potential-energy profiles for the keto form of **3** in the ground (K) and excited (K*) singlet states with respect to the torsional angles around the Ar–CO, N–CO, and Ar–N bonds (AM1/PECI=8 calculation).

the aromatic amide bond (Ar–CO) in the excited state, the potential curve shows the maximum value at 0° and the minimum at 90°. The appearance of the S_1 potential-energy surface indicates that there is no barrier for large-amplitude twisting about the Ar–CO bond. Furthermore, the maximum at 90° in the S_0 state produces a smaller gap between the ground and first excited states. As for the rotation around the amide bond (N–CO) in the S_1 state, the potential-energy curve shows a maximum at 90° and thereby produces an estimated activation barrier of 18.09 kcal mol^{-1}. In the potential-energy profile for rotation around Ar–N in the excited state, we found only one maximum at 105° with an interconversion barrier of 17.54 kcal mol^{-1}. Gelation-induced fluorescence emission in **3** and **4** could then be rationalized and supported by combining these theoretical calculations with the previously reported findings given below: in a rigid matrix at 77 K, the flexible Ar–CO, N–CO, and Ar–N bond rotations are inhibited. The fluorescence intensity increases 45–50 times with respect to that observed at 294 K.[20a] Upon light absorption, the Franck–Condon excited state maintains the enol geometric structure of the fundamental state and then the subsequent intramolecular excited-state proton transfer enol*→*cis*-keto* takes place. In a fluid solution (low viscosity) at 293 K after ESIPT, that is, when the system achieves a *cis*-keto* character, the MO calculations suggest that the most probable rotation involving the keto-rotated species is the Ar–CO bond. Under such conditions, the fluorescence of the *cis*-keto* isomer can be quenched by dynamic internal torsion processes in the excited state leading to the formation of twisted keto*.[21] This species, accessed after ESIPT, involves a twisted intramolecular charge transfer state (TICT), which brings about the fluorescence quenching observed in solution. Accordingly, the fluorescence enhancement in the solid state is due to prevention of TICT by kinetic constraint, which blocks large-amplitude twisting motion. In essence, the enhanced fluorescent behav-

ior of gelators is attributed to its rigid structure, which precludes extensive twisting about the Ar–CO bond along the reaction coordinate.

Conclusion

Low-molecular-weight organogelators **3** and **4** containing salicylanilide-based ESIPT moieties were synthesized and characterized. Highly fluorescent organogels are easily formed in nonpolar solvents such as dodecane and *n*-hexane by virtue of the self-assembled lamellar and hexagonal columnar structures of **3** and **4**, respectively. By combining the results of UV/Vis absorption and photoluminescence studies and DFT and semiempirical (AM1) calculations, the molecular packing model in the gel phase was deduced. The gelators are self-assembled into complex 3D networks, and their aggregation into fibrous superstructures is driven by π-stacking interactions between the central salicylanilide moieties, hydrogen-bonding interactions among the amide groups, and van der Waals interactions among the alkyl groups. Interestingly, the fluorescence emission intensity of the organogels is 10–50-fold higher than that of the solution phase. Nonradiative relaxation via a TICT is reduced in the hydrogen-bonded supramolecular assembly and gel states, and this leads to enhanced ESIPT fluorescence emission.

Experimental Section

General: 1H NMR spectra were recorded on a Jeol JNM-LA300 (300 MHz) spectrometer in $CDCl_3$ or [D_6]acetone with TMS as internal standard. Molar masses of compounds were measured on a Jeol JMS-AX505WA in electron-impact (EI) mode. Elemental contents of compounds were measured with an EA1110 (CE Instruments, Italy). FTIR studies were performed on a Jasco 200 model spectrometer. Solid samples were recorded as intimate mixtures with powdered KBr. Liquid and gel samples were recorded in a liquid cell equipped with CaF_2 windows and a 0.2 mm lead spacer. Data were registered at 2 cm^{-1} resolution with 32 scans. UV/Vis absorption and fluorescence spectra were recorded on Shimadzu UV-1650PC and Shimadzu RF-500 spectrofluorimeter, respectively, with emission and excitation slit width of 3 nm each. Field-emission scanning electron microscopy (FESEM) images were obtained with a JSM-6330F (Jeol). X-ray diffraction studies were performed in transmission mode with Cu K Co radiation by NICEM (Bruker D5005 diffractometer).

2-(2-Hydroxyphenyl)-4*H*-3,1-benzoxazin-4-one (1): Anthranilic acid (10.0 g, 72.9 mmol) and salicylic acid (10.10 g, 73.1 mmol) were dissolved in pyridine (100 mL) and the solution stirred for 30 min. Triphenyl phosphite (72.5 mol, 19.0 mL) was added and the solution was stirred at 100 °C for about 2 h. The reaction mixture was poured into cold water and extracted with dichloromethane. The solution was dried with anhydrous magnesium sulfate. After removal of the solvent, the crude product was purified by column chromatography on silica gel with ethyl acetate/*n*-hexane (1/3). The product was recrystallized from ethanol to give 3.10 g of pure product (yield 18%). ^{1}H NMR ($CDCl_3$, 300 MHz): δ = 12.45 (s, 1H), 8.23 (d, 1H), 8.07 (d, 1H), 7.84 (t, 1H), 7.61 (d, 1H), 7.50 (m, 2H), 7.05 (d, 1H), 6.97 ppm (t, 1H); *m*/*z* (MS-EI) calcd: 239.23; found: 239; elemental analysis calcd (%) for $C_{14}H_9NO_3$: C 70.29, H 3.79, N 5.86; found: C 70.39, H 3.79 N 5.80.

2-(2-Hydroxyphenyl)-6,7-dimethoxy-4*H*-3,1-benzoxazin-4-one (2): 2-Amino-4,5-dimethoxybenzoic acid (5.0 g, 25.3 mmol) and salicylic acid (3.70 g, 26.8 mmol) were dissolved in pyridine (50 mL) and the solution stirred for 30 min. Triphenyl phosphite (7.0 mL, 26.7 mmol) was added to this solution. The mixture was heated to 100 °C for 2 h. The reaction mixture was poured into cold water and extracted with dichloromethane. The solution was dried with anhydrous magnesium sulfate. After removal of the solvent, the crude product was purified by column chromatography on silica gel with ethyl acetate/*n*-hexane (1/4). The product was recrystallized from ethanol to give 2.30 g of pure product (yield 30%). ^{1}H NMR ($CDCl_3$, 300 MHz): δ = 12.40 (s, 1H), 8.08 (d, 1H), 7.55 (s, 1H), 7.46 (t, 1H), 7.00 (m, 3H), 4.05 (s, 3H), 4.01 ppm (s, 3H); *m*/*z* (MS-EI) calcd: 299.28, found 299; elemental analysis calcd (%) for $C_{16}H_{13}NO_5$: C 64.21, H 4.38, N 4.68; found: C 64.26, H 4.40, N 4.55.

***N*-Heptyl-2-(2-hydroxybenzamido)benzamide (3)**: Compound **1** (1.0 g, 4.2 mmol) and *n*-heptylamine (0.60 g, 5.2 mmol) were dissolved in pyridine (50 mL). The solution was heated at 100 °C and refluxed under N_2 atmosphere for 24 h. The reaction mixture was poured into cold water and neutralized with 1 N HCl solution, after which the precipitate was collected by filtration. The crude product was purified by column chromatography on silica gel with ethyl acetate/*n*-hexane (1/10). The product was recrystallized from ethanol to give 1.50 g of pure product (yield 59%). ^{1}H NMR ($CDCl_3$, 300 MHz), δ = 12.37 (s, 1H), 12.34 (s, 1H), 8.67 (d, 1H), 7.80 (d, 1H), 7.52 (m, 2H), 7.43 (t, 1H), 7.16 (t, 1H),7.00 (m, 2H), 6.18 (s, 1H), 3.50 (q, 2H), 1.62 (m, 2H), 1.30 (m, 8H), 0.88 ppm (t, 3H); IR (KBr pellet): $\tilde{\nu}$ = 3300 (ν_{OH} or $_{NH}$), 1655 (ν_{CO}) cm^{-1}; *m*/*z* (MS-EI) calcd: 354.44, found: 354; elemental analysis calcd (%) for $C_{21}H_{26}N_2O_3$: C 71.16, H 7.39, N 7.90; found: C 71.40, H 7.50, N 7.87.

***N*-Heptyl-2-(2-hydroxybenzamido)-4,5-dimethoxybenzamide (4)**: Compound **2** (1.0 g, 3.3 mmol) and *n*-heptylamine (1.0 g, 8.6 mmol) were dissolved in pyridine (30 mL). The solution was heated to reflux at 100 °C for 24 h. The reaction mixture was poured into cold water and neutralized with 1 N HCl solution. The precipitate was collected by filtration. The crude product was purified by column chromatography on silica gel with ethyl acetate/*n*-hexane (1/10). The product was recrystallized from ethanol to give 0.90 g of pure product (yield 65%). ^{1}H NMR ($CDCl_3$, 300 MHz): δ = 12.60 (s, 1H), 12.40 (s, 1H), 8.40 (s, 1H), 7.79 (d, 1H), 7.41 (t, 1H), 7.00–6.92 (m, 3H), 6.23 (s, 1H), 3.99 (s, 3H), 3.89 (s, 3H), 3.46 (q, 2H), 1.63 (m, 2H), 1.34 (m, 8H), 0.86 ppm (t, 3H); ^{13}C NMR ($CDCl_3$, 75 MHz): δ = 168.85, 168.76, 162.01, 152.21, 144.52, 134.65, 134.31, 126.37, 119.23, 118.40, 115.06, 112.23, 109.24, 105.16, 56.43, 56.09, 40.16, 31.67, 29.48, 28.90, 26.92, 22.53, 14.01 ppm; IR (KBr pellet): $\tilde{\nu}$ = 3312 ($_{OH}$ or ν_{NH}), 1650 (ν_{CO}) cm^{-1}; *m*/*z* (MS-EI) calcd: 414.49, found: 414; elemental analysis calcd (%) for $C_{23}H_{30}N_2O_5$: C 66.65, H 7.30, N 6.76; found: C 66.51, H 7.35, N 6.74.

2-Phenyl-4*H*-3,1-benzoxazin-4-one (5): Anthranilic acid (1.0 g, 7.3 mmol) was dissolved in pyridine (20 mL) and the solution stirred for 10 min. Benzoyl chloride (2.05 g, 14.6 mmol) was added to this solution. The solution was stirred for 2 h at room temperature. The reaction mixture was poured into cold water and the precipitate collected by filtration. The crude product was recrystallized from ethanol to give 0.65 g of pure product (yield 40%). ^{1}H NMR ([D_6]acetone, 300 MHz): δ = 8.32 (t, 1H), 8.29 (d, 1H), 8.21 (d, 1H), 7.97 (m, 1H), 7.73 (d, 1H), 7.68–7.61 ppm (m, 4H); *m*/*z* (MS-EI) calcd: 223.23, found: 223; elemental analysis calcd (%) for $C_{14}H_9NO_2$: C 75.33, H 4.06, N 6.27; found: C 75.26, H 4.01, N 6.22.

6,7-Dimethoxy-2-phenyl-4*H*-3,1-benzoxazin-4-one (6): 2-Amino-4,5-dimethoxybenzoic acid (1.0 g, 5.1 mmol) was dissolved in pyridine (20 mL) and stirred for 10 min. Benzoyl chloride (1.4 g, 10.0 mmol) was added to this solution and the mixture was stirred for 2 h at room temperature. The reaction mixture was poured into cold water and the precipitate collected by filtration. The crude product was recrystallized from ethanol to give 0.78 g of pure product (yield 54%).^{1}H NMR ($CDCl_3$, 300 MHz): δ = 8.29 (d, 2H), 7.58–7.51 (m, 4H), 7.13 (s, 1H), 4.05 (s, 3H), 4.01 ppm (s, 3H); *m*/*z* (MS-EI) calcd: 283.28, found: 283; elemental analysis calcd (%) for $C_{16}H_{13}NO_4$: C 67.84, H 4.63, N 4.94; found: C 67.89, H 4.65, N 4.92.

2-Benzamido-*N*-heptylbenzamide (7): Compound **5** (0.5 g, 2.2 mmol) and *n*-heptylamine (0.80 g, 6.9 mmol) were dissolved in pyridine (20 mL). The solution was heated to reflux at 100 °C for 24 h. The reaction mixture was

poured into cold water and neutralized with 1 N HCl. The precipitate was collected by filtration. The crude product was purified by column chromatography on silica gel with ethyl acetate/*n*-hexane (1/10). The product was recrystallized from ethanol to give 0.60 g of pure product (yield 80%). ^{1}H NMR ($CDCl_3$, 300 MHz): $\delta = 12.10$ (s, 1H), 8.79 (d, 1H), 8.04 (d, 2H), 7.55–7.48 (m, 5H), 7.09 (t, 1H), 6.33 (s, 1H), 3.45 (q, 2H), 1.62 (m, 2H), 1.35 (m, 8H), 0.88 ppm (t, 3H); IR (KBr pellet): $\tilde{\nu} = 3340$ (ν_{NH}), 1663 (ν_{CO}) cm^{-1}; *m*/*z* (MS-EI) calcd: 338.44, found 338; elemental analysis calcd (%) for $C_{21}H_{26}N_2O_2$: C 74.52, H 7.74, N 8.28; found: C 74.47, H 7.86, N 8.45.

2-Benzamido-*N*-heptyl-4,5-dimethoxybenzamide (8): Compound **6** (0.30 g, 1.05 mmol) and *n*-heptylamine (0.38 g, 3.2 mmol) were dissolved in pyridine (20 mL). The solution was heated at 100 °C and refluxed for 24 h. The reaction mixture was poured into cold water and neutralized with 1 N HCl solution. The precipitate was collected by filtration. The crude product was purified by column chromatography on silica gel with ethyl acetate/*n*-hexane (1/10). The product was recrystallized from ethanol to give 0.26 g of pure product (yield 62%). ^{1}H NMR ($CDCl_3$, 300 MHz): $\delta = 12.41$ (s, 1H), 8.59 (s, 1H), 8.02 (d, 2H), 7.51 (m, 3H), 6.95 (s, 1H), 6.36 (s, 1H), 3.97 (s, 3H), 3.86 (s, 3H), 3.4 (q, 2H), 1.61 (m, 2H), 1.31 (m, 8H), 0.85 ppm (t, 3H); ^{13}C NMR ($CDCl_3$, 75 MHz): $\delta =$ 168.90, 165.45, 152.23, 144.10, 135.68, 134.75, 131.73, 128.73, 127.22, 111.83, 109.40, 104.72, 56.41, 56.01, 40.09, 31.66, 29.50, 28.90, 26.92, 22.52, 14.00 ppm; IR (KBr pellet): $\tilde{\nu} = 3418$ (ν_{NH}), 1662 (ν_{CO}) cm^{-1}; *m*/*z* (MS-EI) calcd: 398.50, found 398; elemental analysis calcd (%) for $C_{23}H_{30}N_2O_4$: C 69.32, H 7.59, N 7.03; found: C 69.25, H 7.68, N 6.93.

2-(2-Hydroxybenzamido)-4,5-dimethoxybenzoic acid (9): Compound **2** (0.42 g, 1.4 mmol) and KOH (1.0 g) were dissolved in water (10 mL). The solution was stirred for 30 min at 100 °C and then poured into cold water and neutralized with 1 N HCl. The precipitate was collected by filtration. The crude product was purified by column chromatography on silica gel with ethyl acetate/*n*-hexane (1/3). The product was recrystallized from ethanol to give 0.37 g of pure product (yield 83%). ^{1}H NMR ($CDCl_3$, 300 MHz): $\delta = 12.17$ (s, 1H), 12.09 (s, 1H), 8.58 (s, 1H), 7.77–7.73 (d, 1H), 7.57 (s, 1H), 7.48–7.42 (t, 1H). 7.03 (d, 1H), 6.98–6.93 (m, 2H), 4.05 (s, 3H), 3.94 ppm (s, 3H); *m*/ (MS-EI) calcd: 317.29, found: 317.0; elemental analysis calcd (%) for $C_{16}H_{15}NO_6$: C 60.57, H 4.77, N 4.41; found: C 60.68, H 4.62, N 4.29.

Heptyl 2-(2-hydroxybenzamido)-4,5-dimethoxybenzoate (10): Compound **9** (0.25 g, 0.79 mmol) and heptanol (0.28 g, 2.4 mmol) were dissolved in tetrahydrofuran (8 mL). Triphenylphosphine (0.42 g, 1.6 mmol) and DEAD (0.28 g, 1.6 mmol) were added subsequently. The solution was stirred for 24 h at room temperature. The reaction mixture was poured into cold water and extracted with ethyl acetate. The crude product was purified by column chromatography on silica gel with ethyl acetate/*n*-hexane (1/10). The product was recrystallized from ethanol to give 0.20 g of pure product (yield 61%). ^{1}H NMR ($CDCl_3$, 300 MHz): $\delta = 12.39$ (s, 1H), 12.29 (s, 1H), 8.55 (s, 1H), 7.83 (d, 1H), 7.60 (s, 1H), 7.47 (t, 1H), 7.00 (m, 2H), 4.37 (t, 2H), 4.16 (s, 3H), 3.87 (s, 3H), 1.82 (m, 2H), 1.43 (m, 4H), 1.32 (m, 4H), 0.89 ppm (t, 3H); *m*/*z* (MS-EI) calcd: 415.48, found: 415; elemental analysis calcd (%) for $C_{23}H_{29}NO_6$: C 66.49, H 7.04, N 3.37; found: C 66.53, H 6.97, N 3.51.

Preparation of gels and determination of gelation temperatures: Weighed amounts of organogelator were added to the solvent and heated until all organogelators were fully dissolved. The solution was then left to cool to room temperature. The inverted-test-tube method was used to examine gel formation in different solvents and to determine critical gelation concentration (CGC). The dropping-ball method was used to determine the sol–gel phase-transition temperature (T_{gel}).

UV/Vis absorption and photoluminescence (PL): A UV/cell for opaque gel was constructed with 1 mm path length. Photoluminescence of opaque liquids and solids were measured in the same measurement cuvette by the front-face detection technique at an angle that minimizes reflected and scattered light. Photoluminescence quantum efficiencies Φ_{PL} for solutions were obtained by using 9,10-diphenylanthracene as reference,[24] while Φ_{PL} of PMMA film doped with 10 wt% of organogelators **3** or **4** were measured with a six-inch integrating sphere (Labsphere, 3P-GPS-060-SF) equipped with a 325 nm CW HeCd laser (Omnichrome, Series 56) and a PMT detector (Hamamatsu, PD471) attached to a monochromator (Acton Research, Spectrapro-300i). The detailed analytical procedure to obtain solid-state Φ_{PL} has been described elsewhere.[25]

Computational details: DFT calculations were used to obtain the geometries and energetics of the internally hydrogen-bonded organogelator **3**. Becke's three-parameter exact exchange functional (B3)[26] combined with the gradient-corrected correlation functional of Lee–Yang–Parr (LYP)[27] was employed to optimize the conformations of molecules in gaseous phase with the 6-31G** basis set. At the respective ground-state optimized geometries, time-dependent DFT (TDDFT)[28] calculations using the B3LYP functional were performed to obtain vertical excitation energies. Considering the dimer structure of gelator **3** as the first step towards understanding the structure of xerogel, geometries for the dimers were computed with no symmetry restrictions by using the B3LYP functional in combination with the 6-31G** basis set. Frequency calculations were also carried out to ensure that an energy minimum was obtained in each case. The energy of interaction between gelator pairs was calculated as the difference between the energies of the dimer and the individual moieties. All interaction energies calculated by the B3LYP/6-31G** method were corrected for the basis set superposition error (BSSE) by using a standard counterpoise method.[29] The ground-state B3LYP and excited-state TDDFT calculations were carried out with the Gaussian 03 computational package.[30] Since organogelator **4** differs from **3** only in the 4,5-dimethoxy groups at the phenyl ring, time-consuming higher level theoretical calculations were not performed for **4**.

In addition to high-level DFT calculations, semiempirical methods offer an attractive alternative for studying potential-energy surfaces in ground and excited states. Procedures such as the AM1 method[31] allow examination of potential-energy surfaces without geometric assumptions. With inclusion of limited configuration interaction, especially through the single and pair double excitation (PECI) procedure,[32] spectral properties of several conjugated organic systems have been reliably reproduced.[33] Therefore, we simulated the spectral properties of ESIPT gelator **3** using AM1/PECI = 8 calculations in order to guide the synthetic efforts towards materials with enhanced performance and to help interpret the experimental data. The geometry-dependent potential energies in the ground (S_0) and first excited (S_1) states which were calculated by changing geometrical parameters of interest from the optimized geometry. In these calculations, all the geometrical parameters were optimized at each point.

Acknowledgements

This research was supported in parts by Basic Science Research Program through the National Research Foundation of Korea (NRF) funded by the Ministry of Education, Science and Technology (CRI; RIAMI-AM0209(0417-20090011)).

[1] a) P. Terech, R. G. Weiss, *Chem. Rev.* **1997**, *97*, 3133–3159; b) J. H. van Esch, B. L. Feringa, *Angew. Chem.* **2000**, *112*, 2351–2354; *Angew. Chem. Int. Ed.* **2000**, *39*, 2263–2266; c) N. M. Sangeetha, U. Maitra, *Chem. Soc. Rev.* **2005**, *34*, 821–836; d) A. Brizard, R. Oda, I. Huc, *Top. Curr. Chem.* **2005**, *256*, 167–218; e) D. J. Abdallah, R. G. Weiss, *Adv. Mater.* **2000**, *12*, 1237–1247; f) R. J. H. Hafkamp, M. C. Feiters, R. J. M. Nolte, *J. Org. Chem.* **1999**, *64*, 412–426; g) L. A. Estorff, A. D. Hamilton, *Chem. Rev.* **2004**, *104*, 1201–1217; h) F. Fages, *Angew. Chem.* **2006**, *118*, 1710–1712; *Angew. Chem. Int. Ed.* **2006**, *45*, 1680–1682; i) T. Ishi-I, S. Shinkai, *Top. Curr. Chem.* **2005**, *258*, 119–160; j) T. Kato, N. Mizoshita, M. Moriyama, T. Kitamura, *Top. Curr. Chem.* **2005**, *256*, 219–236.

[2] a) M. Ayabe, T. Kishida, N. Fujita, K. Sada, S. Shinkai, *Org. Biomol. Chem.* **2003**, *1*, 2744–2747; b) D. Berthier, T. Buffeteau, J.-M. Léger, R. Oda, I. Huc, *J. Am. Chem. Soc.* **2002**, *124*, 13486–13494; c) M. George, R. G. Weiss, *Langmuir* **2003**, *19*, 1017–1025; d) S. Tanaka, M. Shirakawa, K. Kaneko, M. Takeuchi, S. Shinkai, *Langmuir* **2005**,

21, 2163–2172; e) T. Haino, M. Tanaka, Y. Fukazawa, *Chem. Commun.* **2008**, 468–470.

[3] a) A. R. Hirst, D. K. Smith, M. C. Feiters, H. P. M. Geurts A. C. Wright, *J. Am. Chem. Soc.* **2003**, *125*, 9010–9011; b) K. S. Partridge, D. K. Smith, G. M. Dykes, P. T. McGrail, *Chem. Commun.* **2001**, 319–320; c) K. Hanabusa, T. Miki, Y. Taguchi, T. Koyama, H. Shirai, *J. Chem. Soc. Chem. Commun.* **1993**, 1382–1384; d) Y. Ishihara, H. S. Bazzi, V. Toader, F. Godin, H. F. Sleiman, *Chem. Eur. J.* **2007**, *13*, 4560–4570; e) F. Camerel, L. Bonardi, M. Schmutz, R. Ziessel, *J. Am. Chem. Soc.* **2006**, *128*, 4548–4549; f) C. Wang, D. Zhang, J. Xiang, D. Zhu, *Langmuir* **2007**, *23*, 9195–9200; g) M. Shirakawa, S.-I. Kawano, N. Fujita, K. Sada, S. Shinkai, *J. Org. Chem.* **2003**, *68*, 5037–5044; h) B. Jancy, S. K. Asha, *Chem. Mater.* **2008**, *20*, 169–181.

[4] a) T. H. Kim, M. S. Choi, B.-H. Sohn, S.-Y. Park, W. S. Lyoo, T. S. Lee, *Chem. Commun.* **2008**, 2364–2366; b) M. Hashimoto, S. Ujiie, A. Mori, *Adv. Mater.* **2003**, *15*, 797–800; c) J. Seo, S. Kim, S. H. Gihm, C. R. Park, S. Y. Park, *J. Mater. Chem.* **2007**, *17*, 5052–5057.

[5] a) P. Babu, N. M. Sangeetha, P. Vijaykumar, U. Maitra, K. Rissanen, A. R. Raju, *Chem. Eur. J.* **2003**, *9*, 1922–1932; b) P. Mukhopadhyay, Y. Iwashita, M. Shirakawa, S.-I. Kawano, N. Fujita, S. Shinkai, *Angew. Chem.* **2006**, *118*, 1622–1625; *Angew. Chem. Int. Ed.* **2006**, *45*, 1592–1595; c) A. Friggeri, O. Gronwald, K. J. C. van Bommel, S. Shinkai, D. N. Reinhoudt, *J. Am. Chem. Soc.* **2002**, *124*, 10754–10758.

[6] a) M. Dukh, D. Šaman, J. Kroulík, I. Černy, V. Pouzar, V. Král, P. Drašar, *Tetrahedron* **2003**, *59*, 4069–4076; b) F. Camerel, R. Ziessel, B. Donnio, C. Bourgogne, D. Guillon, M. Schmutz, C. Iacovita, J.-P. Bucher, *Angew. Chem.* **2007**, *119*, 2713–2716; *Angew. Chem. Int. Ed.* **2007**, *46*, 2659–2662; c) J. K.-H. Hui, Y. Zhen, M. J. MacLachlan, *Angew. Chem.* **2007**, *119*, 8126–8129; *Angew. Chem. Int. Ed.* **2007**, *46*, 7980–7983; d) R. Ziessel, G. Pickaert, F. Camerel, B. Donnio, D. Guillon, M. Cesario, T. Prange, *J. Am. Chem. Soc.* **2004**, *126*, 12403–12413.

[7] S. K. Maji, M. G. B. Drew, A. Banerjee, *Chem. Commun.* **2001**, 1946–1947.

[8] A. Aggeli, M. Bell, N. Boden, J. N. Keen, P. F. Knowles, T. C. B. Mcleish, M. Piteathly, S. E. Radford, *Nature* **1997**, *386*, 259–262.

[9] O. Terech, E. Ostuni, R. G. Weiss, *J. Phys. Chem.* **1996**, *100*, 3759–3766.

[10] a) A. T. Polishuk, *J. Am. Soc. Lubr. Eng.* **1977**, *33*, 133–138; b) W. Klyne, *The Chemistry of Steroids*, Wiley, New York, **1960**; c) T. Brotin, R. Utermohlen, F. Fages, H. Bouas-Laurent, J. P. Desvergne, *J. Chem. Soc.* **1991**, 416 –418; d) Y. C. Lin, R. G. Weiss, *Macromolecules* **1987**, *20*, 414–417.

[11] a) V. K. Praveen, S. J. George, R. Varghese, C. Vijayakumar, A. Ajayaghosh, *J. Am. Chem. Soc.* **2006**, *128*, 7542–7550; b) A. Del Guerzo, A. G. L. Olive, J. Reichwagen, H. Hopf, J.-P. Desvergne, *J. Am. Chem. Soc.* **2005**, *127*, 17984–17985; c) J. H. Jung, S. J. Lee, J. A. Rim, H. Lee, T.-S. Bae, S. S. Lee, S. Shinkai, *Chem. Mater.* **2005**, *17*, 459–462.

[12] a) A. Ajayaghosh, V. K. Praveen, C. Vijayakumar, *Chem. Soc. Rev.* **2008**, *37*, 109–122; b) P. Xue, R. Lu, G. Chen, Y. Zhang, H. Nomoto, M. Takafuji, H. Ihara, *Chem. Eur. J.* **2007**, *13*, 8231–8239.

[13] a) H. Maeda, Y. Haketa, T. Nakanishi, *J. Am. Chem. Soc.* **2007**, *129*, 13661–13674; b) C. Bao, R. Lu, M. Jin, P. Xue, C. Tan, G. Liu, Y. Zhao, *Org. Biomol. Chem.* **2005**, *3*, 2508–2512.

[14] L. Guo, Q.-L. Wang, Q.-Q. Jiang, Q.-J. Jiang, Y.-B. Jiang, *J. Org. Chem.* **2007**, *72*, 9947–9953.

[15] a) S. Kamath, J. K. Buolamwini, *Med. Res. Rev.* **2006**, *26*, 569–594; b) C. Liechti, U. Séquin, G. Bold, P. Furet, T. Meyer, P. Traxler, *Eur. J. Med. Chem.* **2004**, *39*, 11–26; c) K. Waisser, O. Bureš, P. Holý, J. Kuneš, R. Oswald, L. Jirásková, M. Pour, V. Klimešová, L. Kubicová, J. Kaustová, *Arch. Pharm. Pharm. Med. Chem.* **2003**, *336*, 53–71; d) M. K. Dahlgren, A. M. Kauppi, I.-M. Olsson, A. Linusson, M. Elofsson, *J. Med. Chem.* **2007**, *50*, 6177–6188; e) J. P. Boyee, M. E. Brown, W. Chin, J. N. Fitzner, R. J. Paxton, M. Shen, T. Stevens, M. F. Wolfson, C. D. Wright, *Bioconjugate Chem.* **2008**, *19*, 1775–1785.

[16] a) S. K. Samanta, A. Pal, S. Bhattacharya, *Langmuir* **2009**, *25*, 8567–8578; b) H. Basit, A. Pal, S. Sen, S. Bhattacharya, *Chem. Eur. J.* **2008**, *14*, 6534–6545; c) S. Bhattacharya, S. N. G. Acharya, *Chem. Mater.* **1999**, *11*, 3121–3132; d) A. Pal, Y. K. Ghosh, S. Bhattacharya, *Tetrahedron* **2007**, *63*, 7334–7348; e) S. Bhattacharya, S. N. G. Acharrya, A. R. Raju, *Chem. Commun.* **1996**, 2101–2102.

[17] a) T. Kar, S. Debnath, D. Das, A. Shome, P. K. Das, *Langmuir* **2009**, *25*, 8639–8648; b) G. Palui, A. Banerjee, *J. Phys. Chem. B* **2008**, *112*, 10107–10115; c) N. Zweep, A. Hopkinson, A. Meetsma, W. R. Browne, B. L. Feringa, J. H. van Esch, *Langmuir* **2009**, *25*, 8802–8809; d) Y. Mindo, *Spectrochim. Acta A* **1973**, *29*, 431–438; e) J. Peng, K. Liu, X. Liu, H. Xia, J. Liu, Y. Fang, *New J. Chem.* **2008**, *32*, 2218–2224; f) M. Teng, G. Kuang, X. Jia, M. Gao, Y. Li, Y. Wei, *J. Mater. Chem.* **2009**, *19*, 5648–5654; g) L. Lu, T. M. Cocker, R. E. Bachman, R. G. Weiss, *Langmuir* **2000**, *16*, 20–34.

[18] D. J. Abdallah, S. A. Sirchiro, R. G. Weiss, *Langmuir* **2000**, *16*, 7558–7561.

[19] K. Sakurai, Y. Jeong, K. Koumoto, A. Friggeri, O. Gronwald, S. Sakurai, S. Okamoto, K. Inoue, S. Shinkai, *Langmuir* **2003**, *19*, 8211–8217.

[20] a) F. D. Lewis, W. Liu, *J. Phys. Chem. A* **2002**, *106*, 1976–1984; b) F. D. Lewis, T. M. Long, *J. Phys. Chem. A* **1998**, *102*, 5327–5332; c) I. Azumaya, H. Kagechika, Y. Fujiwara, M. Itoh, K. Yamaguchi, K. Shudo, *J. Am. Chem. Soc.* **1991**, *113*, 2833–2838.

[21] a) V. C. Vargas, *J. Phys. Chem. A* **2004**, *108*, 281–288; b) M. Z. Zgierski, A. Grabowska, *J. Chem. Phys.* **2000**, *112*, 6329–6337; c) C. Okabe, T. Nakabayashi, Y. Inokuchi, N. Nishi, H. Sekiya, *J. Chem. Phys.* **2004**, *121*, 9436–9442; d) M. I. Knyazhansky, A. V. Metelitsa, A. J. Bushkov, S. M. Aldoshin, *J. Photochem. Photobiol. A* **1996**, *97*, 121–126.

[22] a) S. Bhattacharya, S. K. Samanta, *Langmuir* **2009**, *25*, 8378–8381; b) P. Chen, R. Lu, P. Xue, T. Xu, G. Chen, Y. Zhao, *Langmuir* **2009**, *25*, 8395–8399.

[23] A. L. Sobolewski, W. Domcke, *Chem. Phys.* **1994**, *184*, 115–124.

[24] I. B. Berlman, *Handbook of Fluorescence Spectra of Aromatic Molecules*, Academic Press, New York, **1971**.

[25] J. C. de Mello, H. F. Wittmann, R. H. Friend, *Adv. Mater.* **1997**, *9*, 230–232.

[26] a) A. D. Becke, *J. Chem. Phys.* **1993**, *98*, 5648–5652; b) A. D. Becke, *Phys. Rev. A* **1988**, *38*, 3098–3100.

[27] C. Lee, W. Yang, R. G. Parr, *Phys. Rev. B* **1988**, *37*, 785–789.

[28] a) C. Jamorski, M. E. Casida, D. R. Salahub, *J. Chem. Phys.* **1996**, *104*, 5134–5147; b) M. Petersilka, U. J. Grossmann, E. K. U. Gross, *Phys. Rev. Lett.* **1996**, *76*, 1212–1215; c) R. Bauernschmitt, R. Ahlrichs, F. H. Hennrich, M. M. Kappes, *J. Am. Chem. Soc.* **1998**, *120*, 5052–5059; d) M. E. Casida, *J. Chem. Phys.* **1998**, *108*, 4439–4449; e) R. E. Stratmann, G. E. Scuseria, M. J. Frisch, *J. Chem. Phys.* **1998**, *109*, 8218–8224.

[29] a) S. Simon, M. Duran, J. J. Dannenberg, *J. Chem. Phys.* **1996**, *105*, 11024–11031; b) S. F. Boys, F. Bernardi, *Mol. Phys.* **1970**, *19*, 553–566.

[30] Gaussain 03, Revision B.03, M. J. Frisch, G. W. Trucks, H. B. Schlegel, G. E. Scuseria, M. A. Robb, J. R. Cheeseman, J. A. Montgomery, Jr., T. Vreven, K. N. Kudin, J. C. Burant, J. M. Millam, S. S. Iyengar, J. Tomasi, V. Barone, B. Mennucci, M. Cossi, G. Scalmani, N. Rega, G. A. Petersson, H. Nakatsuji, M. Hada, M. Ehara, K. Toyota, R. Fukuda, J. Hasegawa, M. Ishida, T. Nakajima, Y. Honda, O. Kitao, H. Nakai, M. Klene, X. Li, J. E. Knox, H. P. Hratchian, J. B. Cross, C. Adamo, J. Jaramillo, R. Gomperts, R. E. Stratmann, O. Yazyev, A. J. Austin, R. Cammi, C. Pomelli, J. W. Ochterski, P. Y. Ayala, K. Morokuma, G. A. Voth, P. Salvador, J. J. Dannenberg, V. G. Zakrzewski, S. Dapprich, A. D. Daniels, M. C. Strain, O. Farkas, D. K. Malick, A. D. Rabuck, K. Raghavachari, J. B. Foresman, J. V. Ortiz, Q. Cui, A. G. Baboul, S. Clifford, J. Cioslowski, B. B. Stefanov, G. Liu, A. Liashenko, P. Piskorz, I. Komaromi, R. L. Martin, D. J. Fox, T. Keith, M. A. Al-Laham, C. Y. Peng, A. Nanayakkara, M. Challacombe, P. M. W. Gill, B. Johnson, W. Chen, M. W. Wong, C. Gonzalez, J. A. Pople, Gaussian Inc., Pittsburgh, PA, **2003**.

[31] a) M. J. S. Dewar, E. G. Zoebisch, E. F. Healy, J. J. P. Stewart, *J. Am. Chem. Soc.* **1985**, *107*, 3902–3909; b) G. B. Rocha, R. O. Freire, A. M. Simas, J. J. P. Stewart, *J. Comput. Chem.* **2006**, *27*, 1101–1111.

[32] a) T. Clark, J. Chandrasekhar, *Isr. J. Chem.* **1993**, *33*, 435–448; b) G. Rauhut, T. Clark, T. Steinke, *J. Am. Chem. Soc.* **1993**, *I15*, 9174–9181.

[33] a) H. Mishra, S. Maheshwary, H. B. Tripathi, N. Sathyamurthy, *J. Phys. Chem. A* **2005**, *109*, 2746–2754; b) V. Misra, H. Mishra, *J. Chem. Phys.* **2008**, *128*, 244701–244708; c) R. Misra, A. Mandal, M. Mukhopadhyay, D. K. Maity, P. Bhattacharyya, *J. Phys. Chem. B* **2009**, *113*, 10779–10791; d) S. Mitra, R. Das, S. P. Bhattacharyya, S. Mukherjee, *J. Phys. Chem. A* **1997**, *101*, 293–298; e) S. Bakalova, J. Kaneti, *Spectrochim. Acta Part A* **2000**, *56*, 1443–1452.

Received: September 23, 2009

Please note: Minor changes have been made to this manuscript since its publication in *Chemistry–A European Journal* Early View. The Editor.

Published online: May 20, 2010

